RICE UNIVERSITY

FAILURE THEORY FOR RED BLOOD CELLS IN COUETTE FLOW

by

Jack A. Jones

A THESIS SUBMITTED
IN PARTIAL FULFILLMENT OF THE
REQUIREMENTS FOR THE DEGREE OF

Master of Science

Thesis Director's Signature:

Houston, Texas

May, 1973

ABSTRACT

FAILURE THEORY FOR RED BLOOD
CELLS IN COUETTE FLOW

by

Jack A. Jones

In this analysis, the red blood cell is idealized as a spherical liquid drop, encapsulated by a thin membrane. By transforming G. I. Taylor's equations for the surface loading on a liquid drop with no membrane in Couette flow, spherical loading components are calculated for a drop with a membrane. A solution developed by Flügge for unsymmetrical loading of spherical shells is then used to derive the complete membrane stress pattern for spherical, membrane-encapsulated, liquid drops in Couette flow. The maximum distortion energy is calculated for any given shear rate, and using the relation, a critical shear stress for short duration failure is found as a function of the critical distortion energy.

Viscoelastic solutions based on the maximum normal strain failure theory and the maximum stress failure theory are then developed in order to predict the entire critical shear stress vs. time curve for hemolysis. Using data supplied by Rand's micropipette experiments on red cell membrane

strength, the theories are then shown to roughly predict the entire couette flow hemolysis curve for times up to 10^2 seconds.

Thus, the theory in this analysis provides a much greater understanding of the mechanism causing red blood cell damage in artificial heart valves, heart-lung machines, artificial kidneys, etc. In addition, due to the model cell's physical generality, the theory is applicable to other biological and non-biological systems.

TABLE OF CONTENTS

ACKNOWLEDGEMENTS

The author wishes to express his appreciation to Dr. J. D. Hellums for his guidance and assistance in this study, and to Byron J. Leverett for his ever-willing help to promote a successful thesis.

The author also wishes to recognize the fellowships and tuition grants provided by the National Science Foundation, Rice University, and the National Institute of Health.

Finally, the author wishes to make special acknowledgement to his friends for their close companionship and support during his stay at Rice.

NOMENCLATURE

English Letters

a	Radius of sphere
A_{-3}	Function defined by Equation (15)
B_{-3}	Function defined by Equation (16)
E	Young's Modulus in Figures 2-A and 2-B
F	Normal force on membrane
ℓ	Membrane thickness
n	Coefficient of Fourier series expansion
$N_\phi, N_\theta, N_{\phi\theta}$	Surface Tensions
P_s	Internal static pressure
p_x, p_y, p_z	Rectangular loading components
p_r, p_ϕ, p_θ	Spherical loading components
p_1, p_2, q_1, q_2	Viscoelastic constants defined by Equation (121)
q_o'', q_1'', q_2''	Young's modulus and dashpot viscosities in Figures 2-A and 2-B
Q	Membrane distortion energy
r	Spherical radius coordinate
t	Time
u, v	Velocity components in x and y directions respectively

U,V	Functions defined by Equations (44) and (45)
W	Membrane distortion energy per volume x $(3E/1+\nu)$
x,y,z	Rectangular coordinates for couette flow
x',y'	Rectangular coordinates for hyperbolic flow

Greek Letters

α	Shear rate
β,γ	Functions defined by Equations (14) and (13)
ε	Strain
θ,ϕ	Spherical angular coordinates defined by Equations (7,8,9)
μ	External fluid viscosity
μ'	Internal fluid viscosity
ν	Poisson's ratio
σ	Membrane stress
σ_1	Membrane stress defined by Equation (102)
τ	Fluid shear stress
ω	Angular velocity of sphere
Φ	Hyperbolic flow potential

Subscripts

c	Critical, i.e. denoting hemolysis
n	Coefficient of Fourier series expansion
N	Normal

o	Refers to time = 0
s	Static
t	Arbitrary time

I. INTRODUCTION

Red blood cell damage and destruction has been associated with the flow of blood through artificial heart valves, heart-lung machines, and artificial kidneys. Significant hemolysis has been observed *in vivo* from prosthetic devices[1-4] and *in vitro* from a variety of other methods.[5-9] It has been shown that at shearing rates near and above the destruction threshold level of 1500 dynes/cm^2 the most important factors in red blood cell hemolysis are the magnitude of the fluid shear stress and the length of exposure time.[10]

In order to present a theoretical study of the mechanism of hemolysis in red blood cells, a model of the red blood cell is chosen so that its physical properties conform closely to that of the erythrocyte under high shear stress. It has been observed[11] that while under shear, red blood cells become prolate ellipsoids with their long axis aligned parallel to the flow direction. The red cell membrane rotates around the liquid hemoglobin interior like a tread of a tank. From microscopic and viscometric results, it has been postulated by several authors[11-14] that mammalian red cells are capable of assuming properties of a fluid drop under shear. The membrane is known to have a high extensional rigidity, but a low bending rigidity,[15] thus allowing for the neglection of bending stress.

As a result of the above observations, the model red blood cell chosen for this analysis is a fluid drop encapsulated by a thin membrane, and the ellipsoid shape is approximated as a sphere. Thus, the tank tread membrane rotation of the ellipsoid is approximated as a solid body rotation of a sphere, i.e. the internal circulation of the hemoglobin is ignored.

Due to the generality of this spherical model, the applications of the failure theory in this thesis extend beyond just the red blood cell. The theory may also be used to predict industrial, liquid-filled, microcapsule failure. These small, spherical microcapsules, which are encapsulated by a thin membrane, are currently being used for a variety of purposes: removal of body urea,[16] blood flow modeling,[17] encapsulation of vile-tasting medicines and corrosive industrial liquids,[18] image reproduction,[19] etc. The theory may also be used to predict the failure of other specific biological systems such as the small, spherical, liquid-filled eggs described by Mitchison and Swann.[20]

II. BACKGROUND

The failure theory chosen to predict short duration hemolysis is known as the distortion energy failure theory, which is the most widely accepted and accurate theory for predicting failure of a ductile material.[21] It is based upon the concept that any elastic material when deformed acquires a certain elastic energy associated with the loading and the resulting strain. Failure occurs when the elastic energy reaches some critical value.

For time durations of stress exceeding a few seconds, the red cell membrane is not completely elastic, but also possesses a liquid-like viscous characteristic similar to Figure 2-B.[22] The failure theory chosen for arbitrary critical time durations, then, cannot be the distortion energy theory. Two other failure criteria, the maximum stress failure theory and the maximum normal strain failure theory are discussed. The maximum stress failure theory, although more commonly used for brittle failure, provides a simple solution to the viscoelastic problem. The maximum normal strain theory, which has been postulated from empirical observations,[22] yields a somewhat more complicated solution.

Other attempts to predict red cell membrane failure

have been done by Ultman,[23] Blackshear,[24] and Bernstein et al.[25] Ultman uses a distortion energy failure theory based on a three parameter viscoelastic membrane model (Figure 2-A). His theory is used only in predicting red blood cell micropipette loading failure. On the other hand, Blackshear's theory, which relies on a maximum stress criteria, is actually used for predicting couette flow hemolysis. His theory, however, does not predict a zero time critical fluid shear stress and is applied only for turbulent flow.

Bernstein[25] implies that G. I. Taylor's failure theory[26] for liquid drops in couette flow can be used directly to predict a critical turbulent flow membrane tension, which compares closely with Rand's critical membrane tension of τ_{c_o} = 28.6 dynes/cm. Bernstein, however, does not distinguish between the 1% hemolysis of Blackshear's experiments and the implied 50% hemolysis of Rand's experiments, nor does he note a difference between Blackshear's turbulent jet shear and Taylor's laminar flow shear. In addition, it will be shown that when a membrane encapsulates a liquid drop, the internal pressure is always larger than the external pressure for couette flow, Thus, G. I. Taylor's failure theory, which is based upon equalization of internal and external pressures at high shear, is invalid for direct application to the red blood cell.

III. MEMBRANE SURFACE TENSION SOLUTION

A. Spherical Loading Components

In this section, the couette flow spherical loading components on the model sphere will be calculated as a function of both the position on the membrane's surface and the magnitude of the fluid shear stress, $\alpha\mu$.

Einstein's theoretical treatment[27] of the viscosity of a suspension of rigid spherical particles in a liquid was extended by Taylor[26] to the case of small immiscible fluid spheres. As part of his solution, Taylor calculated the external loading on a fluid sphere due to hyperbolic flow. He further stated that hyperbolic flow is identical to that of couette flow except for a rotation of the whole field (Appendix). Thus, the dynamic forces involved are identical.

Taylor calculates the rectangular surface stress components on a sphere in couette flow as

$$\frac{ap_x}{\mu} = \gamma x - \beta a^{-2}\, x(x^2-y^2) \tag{1}$$

$$\frac{ap_y}{\mu} = -\gamma y - \beta a^{-2}\, y(x^2-y^2) \tag{2}$$

$$\frac{ap_z}{\mu} = -\beta a^{-2}\, z(x^2-y^2) \tag{3}$$

Elementary trigonometric consideration shows that these rectangular components may be expressed in spherical form by means of the following transformation:[28]

$$p_r = \sin \phi \cos \theta \, p_x + \sin \phi \sin \theta \, p_y + \cos \phi \, p_z \quad (4)$$

$$p_\phi = \cos \phi \cos \theta \, p_x + \cos \phi \sin \theta \, p_y - \sin \phi \, p_z \quad (5)$$

$$p_\theta = -\sin \theta \, p_x + \cos \theta \, p_y \quad (6)$$

where the spherical coordinates, Figure 1, for the above transformation are defined by

$$x = a \sin \phi \cos \theta \quad (7)$$

$$y = a \sin \phi \sin \theta \quad (8)$$

$$z = a \cos \phi \quad (9)$$

Substituting p_x, p_y, and p_z into Equations (4-6) and transforming x, y, and z into spherical coordinates by means of Equations (7-9),

$$p_r = \mu(\gamma-\beta) \sin^2 \phi \cos 2\theta \quad (10)$$

$$p_\phi = 1/2 \, \mu\gamma \sin 2\phi \cos 2\theta \quad (11)$$

$$p_\theta = -\mu\gamma \sin \phi \sin 2\theta \, . \quad (12)$$

Taylor[26] defines γ and β as follows:

$$\gamma = A_{-3} - 16B_{-3} + \alpha \tag{13}$$

$$\beta = 4A_{-3} - 40B_{-3} \tag{14}$$

where

$$A_{-3} = \frac{-5\alpha}{2}\left(\frac{\mu' + \frac{2}{5}\mu}{\mu'+\mu}\right) \tag{15}$$

and

$$B_{-3} = \frac{-\alpha}{4}\frac{\mu'}{\mu'+\mu} \quad . \tag{16}$$

Because a membrane is assumed to completely inhibit internal circulation, the red blood cell model will act as a solid sphere in couette flow, i.e.

$$\mu' \to \infty \tag{17}$$

Substituting Equation (17) into Equations (15) and (16) respectively,

$$\lim_{\mu'\to\infty} A_{-3} = \frac{-5\alpha}{2} \tag{18}$$

$$\lim_{\mu'\to\infty} B_{-3} = \frac{-\alpha}{4} \tag{19}$$

Thus, Equations (13) and (14) become

$$\gamma = \frac{5\alpha}{2} \tag{20}$$

and

$$\beta = 0 \tag{21}$$

for a liquid drop encapsulated by a membrane. Substituting these values of γ and β into Equations (10-12),

$$p_r = \frac{5}{2} \alpha\mu \sin^2 \phi \cos 2\theta \tag{22}$$

$$p_\phi = \frac{5}{4} \alpha\mu \sin 2\phi \cos 2\theta \tag{23}$$

$$p_\theta = \frac{-5}{2} \alpha\mu \sin \phi \sin 2\theta \tag{24}$$

B. General Flügge Shell Solution

Flügge[29] has developed a general solution for stresses in spherical shells loaded unsymmetrically. The basic system to be solved consists of three equations in three unknowns (N_ϕ, N_θ, $N_{\phi\theta}$):

$$\frac{\partial}{\partial\phi} (rN_\phi) + a \frac{\partial N_{\theta\phi}}{\partial\theta} - aN_\theta \cos \phi + p_\phi ra = 0 \tag{25}$$

$$\frac{\partial}{\partial\phi} (rN_{\phi\theta}) + a \frac{\partial N_\theta}{\partial\theta} + aN_{\theta\phi} \cos \phi + p_\theta ra = 0 \tag{26}$$

$$\frac{N_\phi}{a} + \frac{N_\theta}{a} = p_r \tag{27}$$

Flügges general solution is summarized as follows. Equation (27) may be used to eliminate N_θ from equations (25) and (26):

$$\frac{\partial N_\phi}{\partial \phi} \sin \phi + 2N_\phi \cos \phi + \frac{\partial N_{\phi\theta}}{\partial \theta} = -a(p_\phi \sin \phi - p_r \cos \phi) \tag{28}$$

$$\frac{\partial N_{\phi\theta}}{\partial \phi} \sin \phi + 2N_{\phi\theta} \cos \phi - \frac{\partial N_\theta}{\partial \theta} = -a(p_\theta \sin \phi + \frac{\partial p_r}{\partial \theta}). \tag{29}$$

The load components p_ϕ, p_θ, and p_r are arbitrary functions of ϕ and θ and may thus be represented in the form:

$$p_\phi = \sum_0^\infty p_{\phi n} \cos n\theta + \sum_1^\infty \bar{p}_{\phi n} \sin n\theta \tag{30}$$

$$p_\theta = \sum_1^\infty p_{\theta n} \sin n\theta + \sum_0^\infty \bar{p}_{\theta n} \cos n\theta \tag{31}$$

$$p_r = \sum_0^\infty p_{rn} \cos n\theta + \sum_1^\infty \bar{p}_{rn} \sin n\theta \tag{32}$$

where $p_{\phi n} \ldots \bar{p}_{rn}$ are functions of ϕ only. The first of the two sums in every line is the load which is symmetric with respect to the meridian $\theta = 0$, and the second sum is the antimetric load.

For each fixed but arbitrary integer n, the solution to Equations (28) and (29) is found by picking out one of the symmetric terms,

$$p_\phi = p_{\phi n} \cos n\theta \tag{33}$$

$$p_\theta = p_{\theta n} \sin n\theta \tag{34}$$

$$p_r = p_{rn} \cos n\theta \tag{35}$$

The solution may be written in the form

$$N_\phi = N_{\phi n} \cos n\theta \tag{36}$$

$$N_\theta = N_{\theta n} \cos n\theta \tag{37}$$

$$N_{\phi\theta} = N_{\phi\theta n} \sin n\theta \tag{38}$$

where $N_{\phi n}$, $N_{\theta n}$, and $N_{\phi\theta n}$ are functions of ϕ only. Thus, the general solution for a load which is symmetric with respect to the meridian is

$$N_\phi = \sum_0^\infty N_{\phi n} \cos n\theta \tag{39}$$

$$N_\theta = \sum_0^\infty N_{\theta n} \cos n\theta \tag{40}$$

$$N_{\phi\theta} = \sum_1^\infty N_{\phi\theta n} \sin n\theta \tag{41}$$

and the antimetric solution is found in a similar way.

Substituting Equations (30-32) and Equations (36-38) into Equations (28) and (29) respectively,

$$\frac{dN_{\phi n}}{d\phi} + 2 \cot \phi \cdot N_{\phi n} + \frac{n}{\sin\phi} N_{\phi\theta n} = a(-p_{\phi n} + \cot \phi \cdot p_{rn}) \tag{42}$$

$$\frac{dN_{\phi\theta n}}{d\phi} + 2 \cot \phi \cdot N_{\phi\theta n} + \frac{n}{\sin\phi} N_{\phi n} = a(-p_{\theta n} + \frac{n}{\sin\phi} p_{rn}). \tag{43}$$

Let us define

$$U \equiv N_{\phi n} + N_{\phi\theta n} \tag{44}$$

$$V \equiv N_{\phi n} - N_{\phi\theta n} , \tag{45}$$

and substitute Equations (44) and (45) into the sum and difference of Equations (42) and (43) respectively:

$$\frac{dU}{d\phi} + (2 \cot \phi + \frac{n}{\sin\phi})U = a(-p_{\theta n} - p_{\phi n} + \frac{n+\cos\phi}{\sin\phi} p_{rn}) \tag{46}$$

$$\frac{dV}{d\phi} + (2 \cot \phi - \frac{n}{\sin\phi})V = a(p_{\theta n} - p_{\phi n} - \frac{n-\cos\phi}{\sin\phi} p_{rn} \tag{47}$$

Equation (46) may be thought of as

$$\frac{dU}{d\phi} + p(\phi) \cdot U + q(\phi) = 0 \tag{48}$$

with a similar expression for Equation (47). From Flügge[29] the general solution of Equation (48) is

$$U = [C - \int q \exp(\int p d\phi) d\phi] \cdot \exp(-\int p d\phi) \tag{49}$$

Applying Equation (49) to Equations (46) and (47), the explicit solution is

$$U = \frac{\cot^n \phi/2}{\sin^2 \phi} \left[A_n - a\int \left(p_{\phi n}+p_{\theta n} - \frac{n+\cos\phi}{\sin\phi} p_{rn}\right) \sin^2 \phi \tan^n\left(\frac{\phi}{2}\right) d\phi\right] \quad (50)$$

$$V = \frac{\tan^n \phi/2}{\sin^2 \phi} \left[B_n - a\int \left(p_{\phi n}-p_{\theta n} + \frac{n-\cos\phi}{\sin\phi} p_{rn}\right) \sin^2 \phi \cot^n\left(\frac{\phi}{2}\right) d\phi\right] \quad (51)$$

The constants A_n and B_n may be determined from the boundary conditions.

C. Dynamic Surface Tension Solution

In order to solve for the surface tensions due to the dynamic load, it is first necessary to express p_r, p_ϕ, and p_θ from Equations (22-24) in component series form as in Equations (30-32). This is done by the following equations.

$$p_r = p_{r2} \cos 2\theta \quad (52)$$

$$p_{r2} = \frac{5\alpha\mu}{2} \sin^2 \phi \quad (53)$$

$$p_\phi = p_{\phi 2} \cos 2\theta \quad (54)$$

$$p_{\phi 2} = \frac{5\alpha\mu}{4} \sin 2\phi \quad (55)$$

$$p_\theta = p_{\theta 2} \sin 2\theta \tag{56}$$

$$p_{\theta 2} = \frac{-5\alpha\mu}{2} \sin \phi \tag{57}$$

Since the load is symmetric with respect to the plane with meridian $\theta = 0$, there are no terms containing $\bar{p}_{\phi n}$, $\bar{p}_{\theta n}$, $\bar{p}_{rn}$ from Equations (30-32).

From Equations (52-57), all indices, n, other than $n = 2$ are zero for dynamic loads. Thus, substituting Equations (53), (55), and (57) into Equations (50) and (51) with $n = 2$ yields

$$U = \frac{\cot^2 \phi/2}{\sin^2 \phi} \left[A_2 + \frac{5\alpha\mu a}{2} \left(3 \cos \phi - \frac{3}{2} \cos 2\phi + \cos^3 \phi\right)\right] \tag{58}$$

$$V = \frac{\tan^2 \phi/2}{\sin^2 \phi} \left[B_2 + \frac{5\alpha\mu a}{2} \left(3 \cos \phi + \frac{3}{2} \cos 2\phi + \cos^3 \phi\right)\right] \tag{59}$$

Adding and subtracting Equations (44) and (45) for $n = 2$,

$$N_{\phi 2} = \frac{1}{2} (U+V) \tag{60}$$

$$N_{\phi\theta 2} = \frac{1}{2} (U-V) \tag{61}$$

Furthermore, from Equations (39) and (41), the dynamic membrane tensions are seen to be

$$N_{\phi_{dyn}} = \frac{1}{2}(U+V) \cos 2\theta \tag{62}$$

$$N_{\phi\theta_{dyn}} = \frac{1}{2}(U-V) \sin 2\theta \tag{63}$$

Substituting Equations (58) and (59) into Equations (62) and (63),

$$N_{\phi_{dyn}} = \frac{\cos 2\theta}{2\sin^4\phi}\{A_2 + B_2 + \frac{15\alpha\mu a}{2} \cos 2\phi$$

$$+ 2 \cos \phi[A_2-B_2-5\alpha\mu a(3 \cos \phi+\cos^3 \phi)]$$

$$+ \cos^2 \phi[A_2+B_2+ \frac{15\alpha\mu a}{2} \cos 2\phi]\} \tag{64}$$

$$N_{\phi\theta_{dyn}} = \frac{\sin 2\theta}{2\sin^4\phi}\{A_2-B_2-5\alpha\mu a(3 \cos \phi+\cos^3 \phi)$$

$$+ 2 \cos \phi[A_2+B_2+ \frac{15\alpha\mu a}{2} \cos 2\phi$$

$$+ \cos^2 \phi[A_2-B_2-5\alpha\mu a(3 \cos \phi+\cos^3 \phi)]\} \tag{65}$$

From Flügge,[29] the two constants, A_2 and B_2, may be determined from the condition that the stress resultants assume finite values at $\phi = 0$. Therefore, since the denominator, $2 \sin^4 \phi$, in Equations (64) and (65) approaches zero

as ϕ approaches zero, the numerators must also approach zero as ϕ approaches zero. Thus,

$$\lim_{\phi \to 0}(2 \sin^4 \phi \, N_{\phi_{dyn}}) = (4A_2 - 25\alpha\mu a)\cos 2\theta = 0 \tag{66}$$

$$\lim_{\phi \to 0}(2 \sin^4 \phi \, N_{\phi\theta_{dyn}}) = (4A_2 - 25\alpha\mu a)\sin 2\theta = 0 \tag{67}$$

It is readily seen that for any arbitrary θ, the solution of either Equation (66) or Equation (67) yields

$$A_2 = \frac{25}{4}\alpha\mu a \tag{68}$$

Similarly, for finite values of the stress resultants at $\phi = \pi$,

$$\lim_{\phi \to \pi}(2 \sin^4 \phi \, N_{\phi_{dyn}}) = (4B_2 - 25\alpha\mu a)\cos 2\theta = 0 \tag{69}$$

$$\lim_{\phi \to \pi}(2 \sin^4 \phi \, N_{\phi\theta_{dyn}}) = (-4B_2 + 25\alpha\mu a)\sin 2\theta = 0 \tag{70}$$

For any arbitrary θ, the solution of Equation (69) or (70) is seen to be

$$B_2 = \frac{25}{4}\alpha\mu a \tag{71}$$

Substituting the above values of A_2 and B_2 into Equations (64) and (65) yields, after simplification,

$$N_{\phi_{dyn}} = \frac{5}{2} \alpha\mu a \cos 2\theta \tag{72}$$

$$N_{\phi\theta_{dyn}} = -\frac{5}{2} \alpha\mu a \sin 2\theta \cos \phi \tag{73}$$

Substituting $N_{\phi_{dyn}}$ from Equation (72) and p_r from Equation (22) into Equation (27) yields

$$N_{\theta_{dyn}} = -\frac{5}{2} \alpha\mu a \cos 2\theta \cos^2 \phi \tag{74}$$

D. Static Surface Tension Solution

The static surface tension is the tension resulting from the internal pressure of the model sphere. Due to symmetry,

$$N_{\phi_s} = N_{\theta_s} \tag{75}$$

and

$$N_{\phi\theta_s} = 0 \tag{76}$$

The normal loading component, p_r, is simply the internal static pressure, i.e.

$$p_{r_{static}} = p_s \tag{77}$$

Substituting Equations (75) and (77) into Equation (27),

$$N_{\phi_s} = N_{\theta_s} = \frac{aP_s}{2} \tag{78}$$

E. Combined Surface Tension Solution

Adding the dynamic solution, Equations (72-74), to the static solution, Equations (76) and (78), the total solution is

$$N_\phi = \frac{5}{2}\alpha\mu a \cos 2\theta + \frac{aP_s}{2} \tag{79}$$

$$N_{\phi\theta} = -\frac{5}{2}\alpha\mu a \sin 2\theta \cos \phi \tag{80}$$

$$N_\theta = -\frac{5}{2}\alpha\mu a \cos 2\theta \cos^2 \phi + \frac{aP_s}{2} \tag{81}$$

Since membranes are incapable of sustaining compressive stresses, the internal pressure, P_s, must increase in order to keep $N_\phi \geq 0$ and $N_\theta \geq 0$ for large rates of shear. Thus, if $N_{\phi_{min}} = 0$ and $N_{\theta_{min}} = 0$, then

$$P_s = 5\alpha\mu \tag{82}$$

Substitution of Equation (82) into Equations (79) and (81) yields

$$N_\phi = \frac{5}{2}\alpha\mu a(1+\cos 2\theta) \tag{83}$$

$$N_\theta = \frac{5}{2}\,\alpha\mu a(1-\cos 2\theta\,\cos^2\phi), \tag{84}$$

both of which are seen to be always non-negative.

IV. ELASTIC THEORY (Short Time Duration of Stress)

Rand[22] has shown that the viscous elements (Figure 2-B) in the red blood cell membrane are associated with times exceeding a few seconds. Thus, for short time durations, the model membrane may be considered to be completely elastic, and a distortion energy failure theory is applicable. According to Juvinall,[21]

> Given a knowledge of only the tensile yield strength of a material, [the distortion energy theory] . . . predicts ductile yielding under combined loading with greater accuracy than any other recognized theory.

Since information is available in the literature[22] on red blood cell tensile yield strength, the distortion energy theory is used hereon to predict short duration erythrocyte failure in couette flow.

The membrane stresses resulting from couette flow are obtained by dividing the membrane surface tensions by the membrane thickness, ℓ. Therefore, from Equations (83), (80), and (84) respectively,

$$\sigma_{\phi} = \frac{5}{2\ell} \alpha\mu a(1+\cos 2\theta) \tag{85}$$

$$\sigma_{\phi\theta} = \frac{-5}{2\ell} \alpha\mu a \sin 2\theta \cos \phi \tag{86}$$

$$\sigma_\theta = \frac{5}{2\ell} \alpha\mu a(1-\cos 2\theta \cos^2 \phi) \tag{87}$$

From Juvinall,[21] the potential energy per volume stored in an elastic material due to distortion may be represented by

$$\frac{dQ}{d\ Vol} = \frac{1+\nu}{3E} (\sigma_\theta^2-\sigma_\phi\sigma_\theta+\sigma_\phi^2+3\sigma_{\phi\theta}^2) \ .$$

When the potential energy per volume reaches some critical value for a particular material, the material is theorized to fail. Since the model red blood cell membrane is assumed to consist of the same material as the real red blood cell membrane, Young's modulus, E, and Poisson's ratio, ν, may be dropped from the above equation. The resulting critical parameter may then be represented by

$$W^2 = \sigma_\theta^2 - \sigma_\phi\sigma_\theta + \sigma_\phi^2 + 3\sigma_{\phi\theta}^2 \tag{88}$$

Substituting Equations (85-87) into Equation (95) yields

$$W^2 = \frac{25\alpha^2\mu^2a^2}{4\ell^2} [1+\cos 2\theta \sin^2 \phi+\cos^2 2\theta(1+\cos^2 \phi+\cos^4 \phi)$$

$$+ \sin^2 2\theta(3 \cos^2 \phi)] \tag{89}$$

Note that

$$\cos^2 2\theta(1+\cos^2\phi+\cos^4\phi) + \sin^2 2\theta(3\cos^2\phi)$$

$$= \cos^2 2\theta(1+\cos^2\phi+\cos^4\phi-3\cos^2\phi)$$

$$+ \cos^2 2\theta(3\cos^2\phi) + \sin^2 2\theta(3\cos^2\phi)$$

$$= \cos^2 2\theta(1-\cos^2\phi)^2 + 3\cos^2\phi$$

Thus Equation (89) may be rewritten as

$$W^2 = \frac{25\alpha^2\mu^2a^2}{4\ell^2}[1+\cos 2\theta \sin^2\phi+3\cos^2\phi$$

$$+ \cos^2 2\theta(1-\cos^2\phi)^2] \qquad (90)$$

Since we want to calculate the maximum distortion energy for any given shear rate, it is necessary to maximize W^2 with respect to any given ϕ and θ. When $\cos 2\theta = 1$, all terms in Equation (90) are maximized for any arbitrary ϕ. Thus

$$W^2_{max} = \frac{25\alpha^2\mu^2a^2}{4\ell^2}[3 + \cos^4\phi] \qquad (91)$$

Clearly, $\cos^4\phi = 1$ for W^2_{max}. Thus

$$W^2_{max} = \frac{25\alpha^2\mu^2a^2}{\ell^2}$$

or

$$W_{max} = \frac{5\alpha\mu a}{\ell} \qquad (92)$$

Furthermore, recalling Newton's law of viscosity, the fluid shear stress is

$$\tau = \mu\alpha \tag{93}$$

then,

$$W_{max} = \frac{5\tau a}{\ell} \tag{94}$$

The distortion energy for symmetric biaxial plane stress, i.e.

$$\left.\begin{aligned} \sigma_\phi &= \sigma_\theta = \frac{N}{\ell} \\ \sigma_{\phi\theta} &= 0 \end{aligned}\right\} \tag{95}$$

may be found by using Equation (88). Thus.

$$W = \frac{N}{\ell} \tag{96}$$

If the critical membrane tension, N_c, is known for short duration stress, then the critical membrane energy may be written

$$W_c = \frac{N_{c_o}}{\ell} \tag{97}$$

In considering the failure of the model sphere used to represent the red blood cell, the critical fluid shear stress is that shear stress at which the maximum distortion energy due to couette flow is equal to the statically-

determined critical distortion energy. Thus by equating Equations (94) and (97),

$$\tau_{c_o} = \frac{N_{c_o}}{5a} \tag{98}$$

V. VISCOELASTIC THEORY (Arbitrary Time Duration of Stress)

As can be seen from Equations (85-87), the membrane stress is a function of position. For any ϕ, the membrane stress in either the ϕ or the θ direction can be seen to vary as a function of the sphere's spin rate, ω, in couette flow. Letting $\omega t = \theta$

$$\sigma_\phi = \sigma_1[1 + \cos(2\omega t)] \tag{99}$$

$$\sigma_{\phi\theta} = -\sigma_1 \sin(2\omega t)\cos\phi \tag{100}$$

$$\sigma_\theta = \sigma_1[1 - \cos(2\omega t)\cos^2\phi] \tag{101}$$

where

$$\sigma_1 = \frac{5}{2\ell}\alpha\mu a \tag{102}$$

From Taylor,[26] the sphere's spin rate, ω, is one-half of the couette flow shear rate, α.

Several possible failure theories for the time dependent viscoelastic solution include the maximum shear stress theory, the maximum stress theory, and the maximum normal strain theory. The maximum shear stress theory is the most accurate of these for predicting ductile yielding. Since no data is available in the literature on time-dependent maximum red cell membrane shear stress, however, this theory is

not hereon considered.

As can be seen from Equations (99) and (101), the maximum stress for couette flow loading is

$$\sigma_{max} = 2\sigma_1 \tag{103}$$

If a loading configuration of

$$\left.\begin{aligned} \sigma_\phi &= \sigma_\theta = \frac{N_{c_t}}{\ell} \\ \sigma_{\phi\theta} &= 0 \end{aligned}\right\} \tag{104}$$

is considered, the maximum couette flow membrane stress is the same as the symmetric biaxial plane loading in Equation (104) if

$$\frac{N_{c_t}}{\ell} = 2\sigma_1 \tag{105}$$

Substituting Equations (93) and (102) into Equation (105) yields a critical couette flow shear stress of

$$\tau_{c_t} = \frac{N_{c_t}}{5a} \tag{106}$$

For t = 0, Equation (106) is seen to yield the same critical fluid shear stress, Equation (98), as predicted by the distortion energy theory.

The maximum normal strain theory assumes failure occurs when some critical normal strain is reached. If one considers the viscoelastic models represented in Figure 2, the maximum normal membrane strain due to couette flow loading, Equations (99-102), may be compared to the maximum normal membrane strain due to symmetric biaxial plane stress, Equation (104). Since the viscous elements, labeled q_1'' and q_2'' in Figure 2-B, are associated with times exceeding a few seconds,[22] they are not appreciably affected by rapid sinuosoidal loads characteristic of the spin rates encountered in couette flow. The elastic element, labeled E, however, is affected by rapid sinusoidal loads since there is no viscous damping associated with it. The normal strain for couette flow loading is then the sum of the viscoelastic strain resulting from $\sigma_\phi = \sigma_\theta = \sigma_1$ plus the elastic strain resulting from a particular σ_ϕ and σ_θ, i.e.

$$(\text{Couette } \varepsilon_N) = (\text{Viscoel } \varepsilon_N)_{\sigma_\phi=\sigma_\theta=\sigma_1}$$

$$+ (\text{Elastic } \varepsilon_N)_{\sigma_\phi,\sigma_\theta}.$$

If a particular normal strain is chosen, e.g., ε_{N_ϕ}, then

$$(\text{Elastic } \varepsilon_{N_\phi})_{\sigma_\phi,\sigma_\theta} = \frac{1}{E}[\sigma_\phi - \nu(\sigma_\theta)]$$

Clearly, the maximum normal strain in the ϕ direction occurs for

$\sigma_{\phi_{max}} = 2\sigma_1$ and $\sigma_{\theta_{min}} = 0$. Thus,

$$(\text{Elastic } \varepsilon_N)_{max} = \frac{2\sigma_1}{E} \tag{107}$$

and

$$(\text{Couette } \varepsilon_N)_{max} = (\text{Viscoel } \varepsilon)_{\sigma_\phi=\sigma_\theta=\sigma_1} + \frac{2\sigma_1}{E} \tag{108}$$

The normal strain for symmetric biaxial plane loading, Equation (104), is

$$(\text{Sym load } \varepsilon_N) = (\text{Viscoel } \varepsilon_N)_{\sigma_\phi=\sigma_\theta=\sigma_1} + (\text{Elastic } \varepsilon_N)_{\sigma_\phi=\sigma_\theta=\sigma_1}$$

$$= (\text{Viscoel } \varepsilon_N)_{\sigma_\phi=\sigma_\theta=\sigma_1} + \frac{1}{E}[\sigma_\theta - \nu(\sigma_\theta)] \tag{109}$$

$$= (\text{Viscoel } \varepsilon)_{\sigma_\phi=\sigma_\theta=\sigma_1} + \sigma_1\left(\frac{1-\nu}{E}\right) \tag{110}$$

Comparing Equations (108) and (110),

$$(\text{Couette } \varepsilon_N)_{max} = (\text{Sym load } \varepsilon_N) + \sigma_1\left(\frac{1+\nu}{E}\right) \tag{111}$$

If the maximum normal strain resulting from couette flow is critical, then Equation (111) may be rewritten for arbitrary time. The quantity σ_{1_t} represents the critical couette σ_1,

Equation (102), for some time t. Thus,

$$\varepsilon_{N_c} = \varepsilon_{\sigma_\phi=\sigma_\theta=\sigma_{1_t}} + \sigma_{1_t}\left(\frac{1+\nu}{E}\right) \tag{112}$$

or

$$1 = \frac{\varepsilon_{\sigma_\phi=\sigma_\theta=\sigma_{1_t}} + \sigma_{1_t}\left(\frac{1+\nu}{E}\right)}{\varepsilon_{N_c}} \tag{113}$$

Since there is no viscous strain at time = 0, Equation (107) then represents the critical normal strain with $\sigma_c = \sigma_{1_o}$, i.e.

$$\varepsilon_{N_c} = \frac{2\sigma_{1_o}}{E} \tag{114}$$

Therefore,

$$\frac{\sigma_{1_t}\left(\frac{1+\nu}{E}\right)}{\varepsilon_{N_c}} = \left(\frac{1+\nu}{2}\right)\frac{\sigma_{1_t}}{\sigma_{1_o}} \tag{115}$$

and from Equation (93),

$$\frac{\sigma_{1_t}\left(\frac{1+\nu}{E}\right)}{\varepsilon_{N_c}} = \left(\frac{1+\nu}{2}\right)\frac{\tau_{c_t}}{\tau_{c_o}} \tag{116}$$

Substituting Equation (116) into Equation (113),

$$\frac{\varepsilon_{\sigma_\phi=\sigma_\theta=\sigma_{1_t}}}{\varepsilon_{N_c}} = 1 - \left(\frac{1+\nu}{2}\right)\frac{\tau_{c_t}}{\tau_{c_o}} \quad . \tag{117}$$

Thus

$$\frac{\sigma_{1_t}\left(\frac{1+\nu}{E}\right)}{\varepsilon_{\sigma_\phi=\sigma_\theta=\sigma_{1_t}}} = \frac{(1+\nu)\tau_{c_t}}{2\tau_{c_o}-(1+\nu)\tau_{c_t}} \tag{118}$$

Rewriting Equation (112),

$$\varepsilon_{N_c} = \varepsilon_{\sigma_\phi=\sigma_\theta=\sigma_{1_t}} + \left[\frac{\sigma_{1_t}\left(\frac{1+\nu}{E}\right)}{\varepsilon_{\sigma_\phi=\sigma_\theta=\sigma_{1_t}}}\right]\varepsilon_{\sigma_\phi=\sigma_\theta=\sigma_{1_t}} \tag{119}$$

$$= \varepsilon_{\sigma_\phi=\sigma_\theta=\sigma_{1_t}}\left[\frac{2\tau_{c_o}}{2\tau_{c_o}-(1+\nu)\tau_{c_t}}\right] \tag{120}$$

For symmetric loading, the total biaxial strain may be assumed to be proportional to the load σ for any given time. Thus from Equation (120),

$$\varepsilon_{N_c} = \varepsilon_{\sigma_\phi=\sigma_\theta=\sigma_{2_t}} \tag{121}$$

where

$$\sigma_{2_t} = \sigma_{1_t}\left[\frac{2\tau_{c_o}}{2\tau_{c_o}-(1+\nu)\tau_{c_t}}\right] \quad . \tag{122}$$

If

$$\sigma_{2_t} = \frac{N_{c_t}}{\ell} \tag{123}$$

and

$$\sigma_{1_t} = \frac{5}{2\ell}\,\tau_{c_t} a \tag{124}$$

then Equation (122) becomes

$$\frac{N_{c_t}}{\ell} = \frac{5}{\ell}\,\tau_{c_t} a\left[\frac{\tau_{c_o}}{2\tau_{c_o} - (1+\nu)\tau_{c_t}}\right] \tag{125}$$

or

$$\tau_{c_t} = \frac{2N_{c_t}\tau_{c_o}}{5a\tau_{c_o} + N_{c_t}(1+\nu)} \tag{126}$$

For t = 0, Equation (125) yields

$$\tau_{c_o} = \left(\frac{1-\nu}{5a}\right) N_{c_o} \tag{127}$$

which is somewhat different than the shear stress predicted by the distortion energy and maximum stress theories. Substituting Equation (127) into Equation (126) yields

$$\tau_{c_t} = \left(\frac{2}{5a}\right)\left[\frac{N_{c_t} N_{c_o}(1-\nu)}{N_{c_o}(1-\nu) + N_{c_t}(1+\nu)}\right] \tag{128}$$

VI. SUBSTITUTION OF EXPERIMENTAL RESULTS

Rand[22] was able to measure the stress required to rupture the red cell membrane. By means of sucking a red cell partially into a micropipette, he was able to calculate the membrane tension corresponding to any known pressure difference across the membrane. The loading resulting from the micropipette suction was symmetric biaxial plane loading, thus similar to Equations (95). By means of numerous such micropipette experiments, Rand determined that the red blood cell of average strength fails when

$$\frac{1}{N_{c_t}} = 3.5 \times 10^{-2} + 3.9 \times 10^{-2}(1-e^{-8t}) + 1.5 \times 10^{-4}t \qquad (129)$$

Thus, depending on which failure criteria is used, Equation (106) or Equation (128) together with Equation (129) represent the average critical couette flow shear rate for hemolysis of the red blood cell of average strength, i.e. 50% hemolysis.

N_{c_o} may be calculated from Equation (129) with $t = 0$;

$$N_{c_o} = 28{,}6 \ \frac{\text{dynes}}{\text{cm}} \qquad (130)$$

According to Fung,[15] the surface area of a red blood cell is

$$\text{Surf. Area} = 163\ \mu^2$$

Using the surface area equation for a sphere, i.e.

$$\text{Surf. Area} = 4\pi a^2,$$

the equivalent radius for the model red cell is

$$a = 3.60\ \mu \tag{131}$$

Using Fung's red blood cell volume of 87 μ^3, however, yields a somewhat lower equivalent volume radius of 2.75 μ. Since we are primarily interested in membrane surface effects, the equivalent radius resulting from the red blood cell surface area will be used in this analysis, but results will also be discussed for the equivalent volume radius.

Mitchison and Swann[20] used $\nu = 0.5$ for sea urchin egg membranes, as this is the approximate value of Poisson's ratio for rubbery materials. In the absence of other information, $\nu = 0.5$ will hereon be assumed for red blood cell membranes. Thus, substituting Equations (130) and (131) into Equations (106) and (128), the couette flow shear stress for 50% hemolysis is found to be respectively

$$\tau_{c_t} = 556\ N_{c_t} \tag{132}$$

for the maximum stress failure theory, and

$$\tau_{c_t} = 3.18 \times 10^4 \frac{N_{c_t}}{(28.6+3N_{c_t})} \tag{133}$$

for the maximum normal strain failure theory. Both Equations (132) and (133) are graphed in Figure 3 and are tabulated with N_{c_t} from Equation (129) in Table 2.

If one uses a = 2.75 μ instead of a = 3.60 μ, then both Equations (132) and (133) would be 30.9% larger. Or, if the approximation for ν is incorrect by as much as ± 10%, then Equation (132) is unaffected, but Equation (133) becomes

$$\tau_{c_t} = 3.18 \times 10^4 \frac{N_{c_t}}{28.6+3.44N_{c_t}}$$

or

$$\tau_{c_t} = 3.18 \times 10^4 \frac{N_{c_t}}{28.6+2.64N_{c_t}}$$

respectively.

Variations of Rand's empirically determined N_{c_t} would also cause changes in the predicted critical shear stress. A variation of ± 10% in N_{c_t} would cause a ± 10% change in both Equations (132) and (133).

VII. DISCUSSION

As can be seen from Figure 3 and Tables 1 and 2, the theoretical critical couette flow shear stresses for 50% hemolysis are somewhat larger than the empirical critical shear stress for 1% hemolysis. Although very little data has been obtained for 50% hemolysis critical shear stresses, Nevaril et al.[30] have shown that the average critical shear rate for 50% hemolysis during a two minute run is actually 3 times the critical shear rate for 1% hemolysis. Thus τ_c for 50% hemolysis with t = 2 minutes is 4500 dynes/cm^2, which compares with the theoretical value of 6000 dynes/cm^2 using the maximum stress failure theory and 5630 dynes/cm^2 using the maximum normal strain failure theory.

Champion et al.[31] have also done some experiments on red blood cell 50% hemolysis. They added thickening agents, Dextran and Methocel, to produce 5 minute critical shear stresses of 2,200 and 10,000 dynes/cm^2 respectively. These values compare with 4670 and 4960 dynes/cm^2 predicted by the maximum stress failure theory and the maximum normal strain failure theory, respectively, for no additive agents. It is possible that Champion's thickening agents not only increased the blood viscosity, but also changed the membrane properties.

The two dips in the theoretical curves in Figure 3 may be explained by looking at Equation (129) which is implicit to both curves. The first of the two dips corresponds to the stretching of the spring dashpot couple represented by q_o'' and q_1'' in Figure 2-B. The second dip corresponds to the stretching of the dashpot element labeled q_2''. Both theoretical curves dip sharply after about 300 seconds. Unfortunately, no comparable empirical data is presently available in this time range.

Possibly the major cause for any discrepancy between theory and fact may be due to the non-sphericity of the red blood cell. In fact, at rest, the red cell assumes the shape of a biconcave discoid. At high shear rates, however, the red blood cell actually becomes a prolate ellipsoid, thus approaching more closely the shape of a sphere. At very low shear rates, however, the red blood cell membrane does not rotate about the hemoglobin in an ellipsoid shape, but rather the entire blood cell tumbles about in a somewhat random motion.[32] Thus, this theory is not applicable in low shear stress ranges.

Another potential cause for discrepancy between theoretical and experimental results may be fatigue. It is quite possible that for long durations, fatigue may be an important part of the red cell membrane failure mechanism. Since no data is available on red cell membrane fatigue however, this factor has been ignored in this analysis. In addition, the

accuracy of Rand's curve for N_{c_t}, Equation (129), is not exactly known.

The one point in Table 1 which does not correlate with any of the curves in Figure 3 is that of Forstrom and Blackshear's turbulent jet experiments.[33] The critical shear stress between 10^{-2} and 10^{-4} seconds remains relatively constant for both human and canine blood, the properties of which are almost identical.[34] Then at 10^{-6} seconds, the critical shear stress for Forstrom's experiments appears to jump a full order of magnitude. The probable explanation for Forstrom and Blackshear's high critical shear stress value, however, is that forces on a red blood cell in turbulent flow are much different than that in laminar flow. Also, the extremely high acceleration resulting from a time duration of 10^{-6} seconds may add to a different type of failure theory.

It is interesting to note that if one uses G. I. Taylor's liquid drop failure theory[26] directly to predict the entire viscoelastic hemolysis curve, then if internal circulation is assumed to be inhibited, i.e. $\mu' \to \infty$,

$$\tau_{c_t} = \frac{8N_{c_t}}{19a} .$$

Thus the critical couette flow shear stress is slightly more than twice as large as that predicted by the maximum stress theory, Equation (106). As mentioned in the Background, however, Taylor's theory is based upon equalization of internal

and external pressures at high shear. Since it has been shown that the internal pressure is always larger than the external pressure when an encapsulating membrane is present, Taylor's failure theory is not directly applicable to the model red blood cell in this analysis.

In summary, the failure theories presented in this thesis provide a much greater understanding of the mechanism causing red blood cell couette flow hemolysis. The theories are shown to roughly predict the entire critical fluid stress vs. time curve for times up to about 10^2 seconds and possibly beyond. In addition, due to the generality of the chosen red blood cell model, the theory is applicable in predicting the failure of other systems including microcapsules or biological systems such as eggs.

TABLE 1

SUMMARY OF EFFECT OF SHEAR STRESS ON HEMOLYSIS

Type of Exposure	Order of Magnitude of Exposure Time, Secs	Threshold Level of Damage, dynes/cm^2	Reference and Comments
Turbulent jet*	10^{-6}	50,000	Forstram and Blackshear[33] (human)
Oscillating wire**	3.5×10^{-4}	5,600	Williams, Hughes, & Nybor[35] (human and canine)
Oscillating bubble**	6.65×10^{-2}	4,500	Rooney[34] (human and canine)
Capillary flow	1.7×10^{-2}	4,500-7,000	Keshavich & Blackshear[36] (canine blood)
Concentric cylinder	1.5×10^{1}	1,900	MacCallum[37] (human)
Concentric cylinder	1.2×10^{2}	1,500	Leverett et al.[10] (human)

*Exposure time of 10^{-6} represents the turbulent eddy time.

**Exposure time estimated to be the boundary layer length divided by the product of the maximum shear rate and the boundary layer thickness.

TABLE 2

THEORETICAL CURVE POINTS FOR EQUATIONS (132,133)

CORRESPONDING TO 50% HEMOLYSIS

Exposure Time (Sec)	N_{c_t} ($\frac{\text{dynes}}{\text{cm}}$)	τ_{c_1} ($\frac{\text{dynes}}{\text{cm}^2}$)	τ_{c_2} ($\frac{\text{dynes}}{\text{cm}^2}$)
0	28.6	1.59×10^4	7.94×10^3
10^{-4}	28.6	1.59×10^4	7.94×10^3
10^{-3}	28.6	1.59×10^4	7.94×10^3
10^{-2}	26.3	1.46×10^4	7.77×10^3
10^{-1}	17.7	9.83×10^3	6.88×10^3
1	13.5	7.50×10^3	6.21×10^3
10	13.2	7.33×10^3	6.15×10^3
10^2	11.2	6.22×10^3	5.72×10^3
1.2×10^2	10.8	6.00×10^3	5.63×10^3
3.0×10^2	8.40	4.67×10^3	4.96×10^3
10^3	4.46	2.48×10^3	3.38×10^3

τ_{c_1} is from maximum stress failure theory.

τ_{c_2} is from maximum normal strain failure theory.

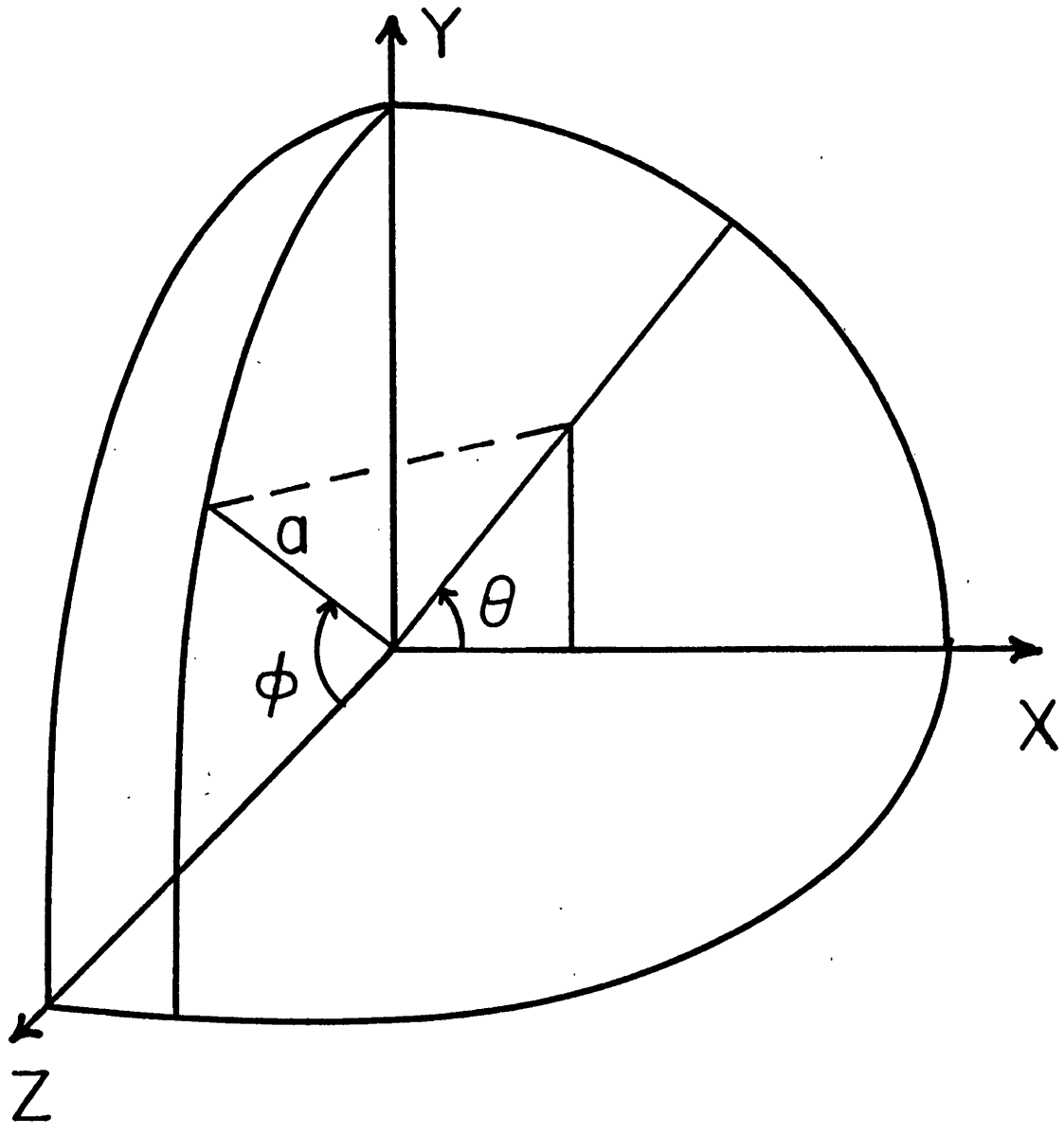

FIGURE 1 - SPHERICAL COORDINATE SYSTEM

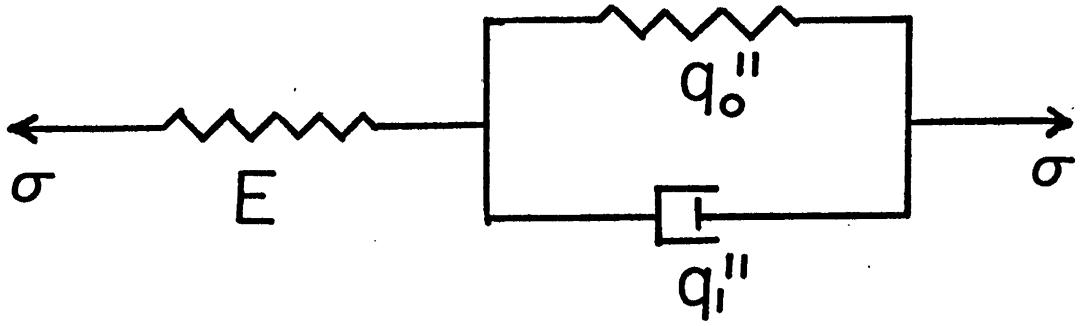

FIGURE 2-A
THREE PARAMETER
VISCOELASTIC MODEL

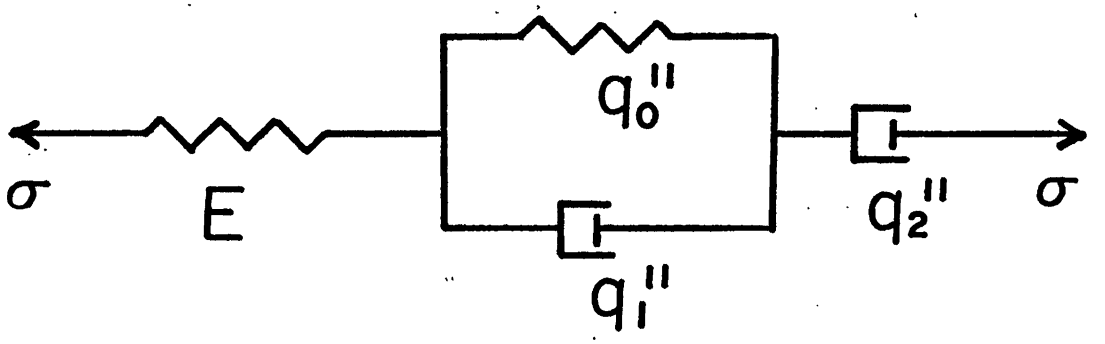

FIGURE 2-B
FOUR PARAMETER
VISCOELASTIC MODEL

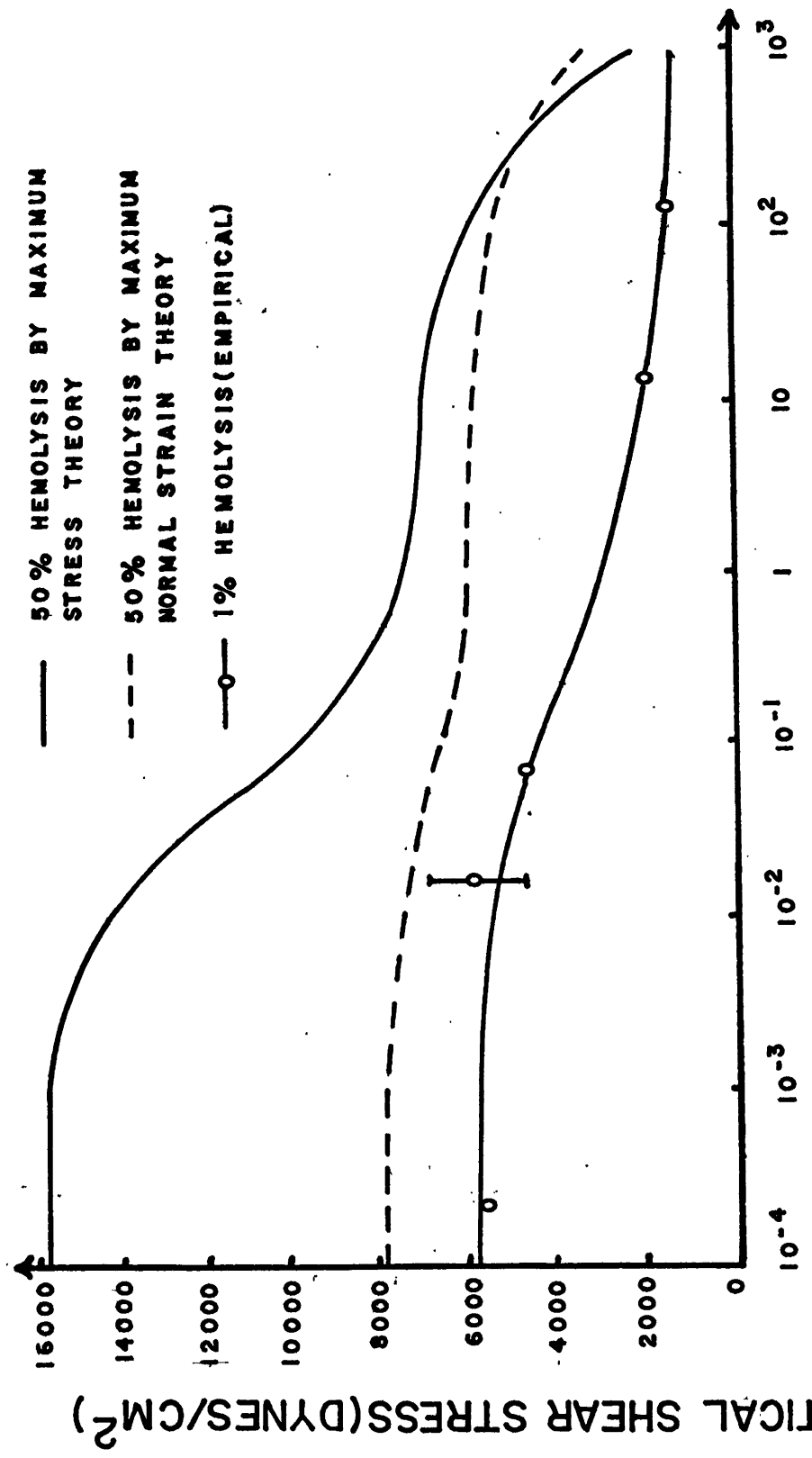

FIGURE 3 - CRITICAL COUETTE FLOW SHEAR STRESS VS. TIME

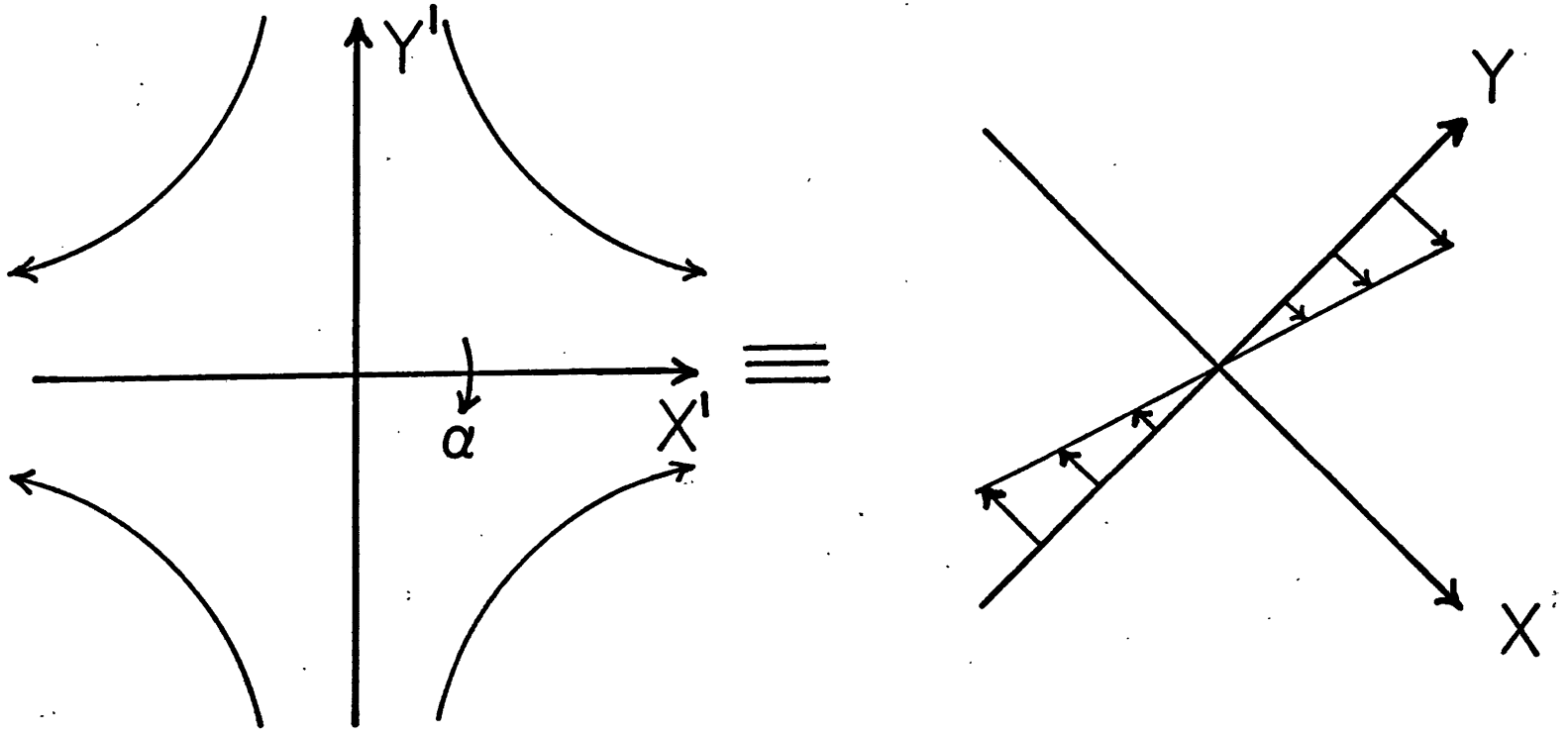

FIGURE 4-TRANSFORMATION OF HYPERBOLIC FLOW(LEFT) TO COUETTE FLOW(RIGHT)

REFERENCES

1. Stevenson, T. D., and H. J. Baker; "Haemolytic Anaemia Following Insertion of Starr-Edwards Valve Prosthesis," Lancet, Vol. 2, p. 982, 1964.

2. Marsh, G. W.; "Intravascular Haemolytic Anemia after Aortic-Valve Replacement," Lancet, Vol. 2, p. 982, 1964.

3. DeCesare, W., C. Rath, and C. Hufnagel; "Hemolytic Anemia of Mechanical Origin with Aortic-Valve Prosthesis," New England Journal of Medicine, Vol. 272, p. 1045, 1965.

4. Sayed, H. M., J. V. Dacie, D. A. Hundley, S. M. Lewis, and W. P. Cleland; Thorax, Vol. 16, p. 356, 1961.

5. Blackshear, P. L., Jr.; "Mechanical Hemolysis in Flowing Blood," Biomechanics; Its Foundations and Objectives, Edited by Y. C. Fung, N. Perrone, and M. Anliker, p. 501, 1971.

6. Nevaril, C. G., J. D. Hellums, C. P. Alfrey, Jr., and E. C. Lynch; "Physical Effects in Red Blood Cell Trauma," AIChE Journal, Vol. 15, p. 707, 1969.

7. Knapp, G. F., and K. A. Yarborough; "An Experimental Investigation of the Mechanism of Hemolysis in Couette Flow," Eighth ICMBE, Chicago, 1969.

8. Shapiro, S. I. and M. C. Williams; "Hemolysis in Simple Shear Flows," AIChE Journal, Vol. 16, p. 575, 1970.

9. Steinbach, J.; M.S. Thesis, University of Minnesota, 1970.

10. Leverett, L. B., J. D. Hellums, C. P. Alfrey, and E. C. Lynch; "Red Blood Cell Damage by Shear Stress," Biophysical Journal, Vol. 12, No. 3, p. 257, 1972.

11. Schmid-Schönbein, H., and R. Wells; "Fluid Drop-Like Transitions of Erythrocytes under Shear," Science, Vol. 165, p. 288, 1969.

12. Dintenfass, L.; "Molecular and Rheological Considerations of the Red Cell Membrane in View of the Internal Fluidity of the Red Cell," Acta Haemotogy, Vol. 32, p. 299, 1964.

13. Dintenfass, L; "Internal Viscosity of the Red Cell and a Blood Viscosity Equation," Nature, Vol. 219, p. 956, 1968.

14. Goldsmith, H. L.; "The Microrheology of Red Blood Cell Suspensions," Journal of General Physiology, Vol. 52, p. 5, 1968.

15. Fung, Y. C.; "Theoretical Considerations of the Elasticity of Red Cells and Small Blood Vessels," Fed. Proc., Vol. 25, p. 1761, 1966.

16. Salemme, R. M., M. H. Litt, Olgierd Lindan, and R. E. Sparks, "Removal of Urea from Solution by Microencapsulated Reactants," Advances in Bioengineering, Vol. 67, No. 114, p. 133.

17. Navarí, R. M., J. L. Gainer, and O. L. Updike, "Blood Flow Modeling with Microcapsular Suspensions," I&EC Fundamentals, Vol. 8, No. 4, p. 615, November 1969.

18. Mattson, Howard,H., "Minature Capsules," International Science and Technology, p. 66, April 1965.

19. "New Way to Make a Tiny Package," Chemical Week, p. 45, January 2, 1965.

20. Mitchison, J. M., and M. M. Swann, "The Mechanical Properties of the Cell Surface, I. The Cell Elastimeter," Journal of Experimental Biology, Vol. 31, No. 3, p. 443, 1954.

21. Juvinall, Robert C., Engineering Considerations of Stress, Strain, and Strength, McGraw-Hill Book Company, 1967.

22. Rand, R. P., "Mechanical Properties of the Red Cell Membrane; II. Viscoelastic Breakdown of the Membrane," Biophysical Journal, Vol. 4, p. 303, 1964.

23. Ultman, J. S.; "The Recoverable Membrane Energy as the Criterion for Hemolysis of the Red Blood Cell," Rheology of Biological Systems, Edited by Henry L. Gabelnick and Mitchell Litt, p. 85, 1973.

24. Blackshear, Perry L., "Mechanical Hemolysis in Flowing Blood," Biomechanics, Its Foundations and Objectives, Edited by Y. C. Fung, N. Perrone, and M. Anliker, Prentice-Hall Inc., p. 501, 1972.

25. Bernstein, E. F., P. F. Blackshear, and K. H. Keller, "Factors Influencing Erythrocyte Destruction in Artificial Organs," American Journal of Surgery, p. 126, July 1967.

26. Taylor, G. I.; "The Viscosity of a Fluid Containing Small Drops of Another Fluid," Proc. Roy. Soc. (London) A138, p. 41, 1932.

27. Einstein, A.; "Eine neue Bestimmung der Molekül-dimensionen," Ann. Physik, Vol. 19, p. 289, 1906; ibid., Vol. 34, p. 591, 1911.

28. Bird, R. Byron, Warren E. Stewart, and Edwin N. Lightfoot; Transport Phenomena, p. 734, 1960.

29. Flügge, Wilhelm, Stresses in Shells, Berlin, Springer, p. 48, 1966.

30. Nevaril, C. G.; "Erythrocyte Damage and Destruction Induced by Shearing Stress," AIChE Journal, Vol. 239, 1972.

31. Champion, J. V., P. F. North, W. T. Coakley, and A. R. Williams; "Shear Fragility of Human Erythrocytes," Biorheology, Vol. 8, p. 23, 1971.

32. Wells, R., and H. Schmid-Schönbein; "Red Cell Deformation and Fluidity of Concentrated Cell Suspensions," Journal of Applied Physiology, Vol. 27, No. 2, 1969.

33. Forstrom, R. J., and P. L. Blackshear, "Fluid Dynamic Lysis of Red Cells," Advances in Bioengineering, 114, 67, p. 69, 1971.

34. Rooney, J. A.; "Hemolysis near an Ultrasonically Pulsating Gas Bubble," Science, Vol. 169, 1970.

35. Williams, A. R., D. E. Hughes, and W. L. Nyborg; "Hemolysis near a Transversly Oscillating Wire," Science, Vol. 169, 1970.

36. Keshavich, Prakash R.; "Hemolysis in Tube Flows at High Shear Rates," Thesis, University of Minnesota, 1970.

37. MacCallum, Robert N.; "Effects of Mechanical Trauma of Normal and Diseased Red Blood Cells," Rice University, Bio-Medical Engineering Laboratory, Report No. 701, 1971.

APPENDIX - Comparison of Hyperbolic Flow to Couette Flow

The velocity potential for hyperbolic flow (Figure 4) is

$$\Phi = \frac{\alpha}{2} [(x')^2 - (y'^2)] \tag{A-1}$$

The flow velocity field may be represented by

$$\bar{v} = \nabla\Phi \tag{A-2}$$

$$= \alpha x'\bar{i} - \alpha y'\bar{j} \tag{A-3}$$

Thus the velocity components are

$$u' = \alpha x' \tag{A-4}$$

$$v' = -\alpha y' \tag{A-5}$$

When the entire field is rotated by an angular velocity of α, then the corresponding additional velocity components are

$$\Delta u' = \alpha y' \tag{A-6}$$

$$\Delta v' = -\alpha x' \tag{A-7}$$

Thus, the new velocity components are

$$u' + \Delta u' = \alpha(x'+y') \tag{A-8}$$

$$v' + \Delta v' = -\alpha(x'+y') \tag{A-9}$$

These components may be expressed in terms of the rotated couette flow coordinate system by means of the following transformation:

$$x' = \frac{1}{\sqrt{2}}(x+y) \tag{A-10}$$

$$y' = \frac{1}{\sqrt{2}}(y-x) \tag{A-11}$$

Substituting Equations (A-10) and (A-11) into Equations (A-8) and (A-9), the hyperbolic velocity components are

$$u' + \Delta u' = \alpha\sqrt{2}\, y \tag{A-12}$$

$$v' + \Delta v' = -\alpha\sqrt{2}\, y \tag{A-13}$$

Or, in terms of velocity components in the x'-y' coordinate system,

$$u = \alpha y \tag{A-14}$$

$$v = 0 \tag{A-15}$$

Since Equations (A-14) and (A-15) also represent the velocity field for couette flow, then it is shown that the rotating hyperbolic flow velocity components are identical to the couette flow velocity components.